analytical chemistry

Article

pubs.acs.org/ac

Dual-Functionalized Porous Si/Hydrogel Hybrid for Label-Free Biosensing of Organophosphorus Compounds

Maksym A. Krepker[†] and Ester Segal*[,†,‡]

[†]Department of Biotechnology and Food Engineering and [‡]The Russell Berrie Nanotechnology Institute, Technion − Israel Institute of Technology, Haifa 32000, Israel

Supporting Information

ABSTRACT: A multifunctional porous Si (PSi) nanostructure is designed to combine a responsive PSi/hydrogel hybrid interfaced with a biorecognition element to selectively recognize small model molecules, organophosphorus compounds (OPCs), of high biological importance. A pH-responsive poly(2-dimethylaminoethyl methacrylate) [poly(DMAEMA)] hydrogel is synthesized and patterned in situ within an oxidized PSi Fabry−Pérot thin film. The resulting new hybrid displays a well-defined, rapid, and reversible optical response to pH changes. We employ this hybrid as an optical transducer element in a biosensing scheme by integrating it with organophosphorus hydrolase (OPH), capable of selective OPC hydrolysis. The enzyme is immobilized onto the pore walls of the oxidized PSi scaffold, resulting in an array of catalytic nanoscale chambers for the degradation of OPCs. Thus, the biosensor function relies on diffusion of the OPCs hydrolysis products from the catalytic chambers, through the interconnected pores network, to the hybrid region triggering its optical response. Exposure to the model target analyte results in a rapid and reproducible change in the optical reflectivity spectrum of the hybrid, allowing for label-free detection and quantification of OPCs in a simple and reliable manner.

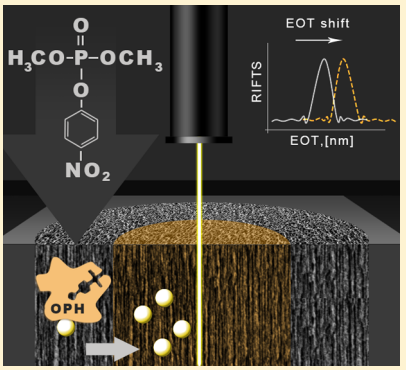

Porous Si (PSi) has emerged over the past decade as a promising nanomaterial for the construction of optical label-free biosensors for various applications.[1−9] The fabrication of PSi by anodic electrochemical etching of a single-crystal Si wafer provides a simple route for building nanostructures with tunable structural and optical properties.[10] Favorable characteristics of PSi for use as optical transducers in biosensing applications include its large surface area and porous volume, compatibility with diverse surface chemistry reactions, and capability for optical readout.[11] A key challenge in PSi biosensors is to effectively stabilize the nanostructure for operating in biological solutions, as PSi oxidation and dissolution in aqueous environments lead to significant signal baseline drifts, signal loss, and ultimately to structural collapse of the PSi thin film.[12−14] Common methods to stabilize PSi nanostructures in aqueous environments (i.e., hydrosilylation or oxidation and subsequent silanization) have shown significant improvements in the material stability.[5,15−19] However, prolonged biosensing experiments in physiological or basic pH conditions continue to demonstrate varying degrees of PSi material corrosion and dissolution, which result in undesirable signal drifts, impeding the widespread use of PSi for biosensing applications.[12,20,21] Our recent work demonstrated that the integration of hydrogels within PSi nanostructures stabilizes the transducer to allow prolonged biosensing experiments in aqueous media[22] in comparison to neat oxidized PSi matrices.[13,23] Hydrogels are three-dimensional cross-linked polymer networks capable of undergoing a reversible volume change in response to different environmental stimuli, such as temperature, pH, electric field, light, and ion strength.[24−28] Thus, their integration with PSi allows for the introduction of new functionalities and responsive behavior.[6,22,29−31] In previous work by Segal et al., temperature and pH responsive PSi/hydrogel hybrids were fabricated by in situ copolymerization of *N*-isopropylacrylamide (NIPAM) and acrylic acid within the porous structure.[29,30] The resulting hybrids exhibit thin-film optical interference spectrum, which enables direct, real-time observation of mechanical and dielectric changes of the nanoconfined hydrogel during its pH-[29] and/or thermally-induced[30,32] volume phase transition. The confined hydrogels undergo a rapid volume phase transition in comparison to the corresponding bulk hydrogels.[29,30,32] Moreover, it was demonstrated that the specific architecture of the oxidized PSi ($PSiO_2$) host directs the kinetics of the hydrogel phase transition. Thus, this new class of responsive hybrids may be engineered to meet the demands of complex systems, such as biosensors, lab-on-chip devices, and drug delivery carriers.[6,33] Herein, we demonstrate this concept by advancing the basic design of PSi/hydrogel hybrids to include a biorecognition interface to selectively recognize and bind small model molecules of high biological importance, organophosphorus compounds (OPCs).

Rapid detection of OPCs in the environment is of great significance for public health protection and for military

Received: April 26, 2013
Accepted: June 24, 2013

   dx.doi.org/10.1021/ac4011815 | *Anal. Chem.* XXXX, XXX, XXX−XXX

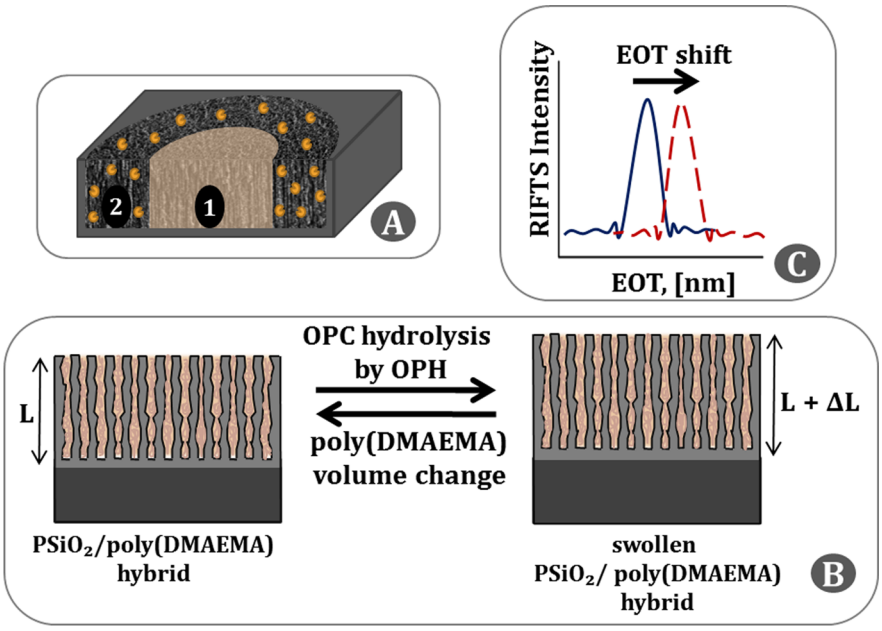

Figure 1. (a) Schematic of the cross section of the biosensor (not drawn to scale). Region 1: $PSiO_2$/poly(DMAEMA) hybrid. Region 2: $PSiO_2$/OPH. (b) Schematic of the $PSiO_2$/poly(DMAEMA) compartment of the biosensor undergoing a volume change due to hydrolysis of the OPC analyte by OPH. (c) Optical response of the device upon the hydrogel volume change.

counterterrorism.[34] OPCs are potent inhibitors of the enzyme acetylcholinesterase (AChE) and their extremely high toxicity is attributed to the excessive cholinergic stimulation caused by inhibition of this enzyme at the neuromuscular junctions and in the central nervous system.[35−37] Synthetic OPCs such as parathion and paraoxon are widely used in agriculture across the world as pesticides, fungicides, and herbicides.[38,39] The World Health Organization reports on three millions cases of OPC-related poisonings worldwide caused by the misuse of these compounds.[37] Thus, rapid and reliable "in-field" detection of OPC is critical.[40−48]

There are several conventional analytical techniques for the detection of OPCs, such as high performance liquid chromatography, gas chromatography, mass spectrometry, and thin layer chromatography, which provide nanomolar detection limits.[36,49−52] However, these methods are laboratory-based, as they require complicated sample preparation by skilled operators and complex instrumentation. Thus, research effort is focused on developing biosensors for real-time in situ detection of OPCs.[53−56] These devices utilize specific enzymes, such as acetylcholinesterase (AChE) and organophosphorus hydrolase (OPH), which have very high affinities for OPCs.[41,43−46,55] Recombinant OPH is a more reliable biological recognition element than AChE, mainly because it is less susceptible to irreversible inhibition by other species; it has a high potential to be reused, and it is more suitable for continuous monitoring.[41,57] OPH is an ∼35 kDa enzyme, capable of reversibly binding OPC and hydrolyzing the organophosphorus triesters at pH 8−10, thereby releasing two protons.[58] Several configurations of OPH-based biosensors, including potentiometric, amperometric, or optical transducers, have demonstrated sensitive detection of OPCs, with a typical response time from minutes to several hours.[41−45,59]

In this work, we present for the first time a biosensor that relies on the responsive behavior of $PSiO_2$/hydrogel hybrids. The biosensor's design comprises of two conjugated interacting compartments, as schematically illustrated in Figure 1a. The first compartment of the biosensor consists of a pH-responsive $PSiO_2$/poly(2-dimethylaminoethyl methacrylate) [poly(DMAEMA)] hybrid and functions as the optical transducer. The second compartment includes the OPH, which is immobilized within the pores of the $PSiO_2$ scaffold, forming an array of catalytic nanoscale chambers used as the biorecognition element. Upon exposure to a model OPC (methyl paraoxon, MOX), the poly(DMAEMA) hydrogel undergoes a volume change (swelling) as a response to a pH decrease induced by the OPH-catalyzed hydrolysis of MOX (Figure 1b). The detection of MOX molecules is optically monitored in real-time using Reflective Interferometric Fourier Transform Spectroscopy (RIFTS)[21,22,30] (Figure 1c). Briefly, the reflectivity spectrum of the $PSiO_2$/hydrogel hybrid is comprised of a series of Fabry-Pérot interference fringes resulting from reflections at the top and bottom interfaces of the thin hybrid material film. The position of the peak along the x axis in the RIFTS spectrum corresponds to the effective optical thickness (EOT), which equals $2nL$ (where n is the effective refractive index and L is the physical thickness of the hybrid film). As changes in n or L occur, they manifest themselves as proportional wavelength shifts in the EOT. Thus, the biosensing concept relies on monitoring changes in the EOT of the $PSiO_2$/poly(DMAEMA) hybrid as a response to OPC hydrolysis by OPH. The resulting multifunctional nanostructure allows for a rapid label-free optical detection and quantification of OPCs.

EXPERIMENTAL SECTION

Preparation of Porous SiO_2. Single-side polished on the ⟨100⟩ face oriented and heavily doped p-type Si (Siltronix Corp.) wafers with an average resistivity of 1 mΩ cm were electrochemically etched in a 3:1 (v/v) solution of aqueous HF (48%, Merck) and absolute ethanol (Merck) for 30 s at a constant current density of 385 mA cm^{-2}. Caution: HF is a highly corrosive liquid and should be handled with extreme

dx.doi.org/10.1021/ac4011815 | Anal. Chem. XXXX, XXX, XXX−XXX

care. Si wafers with an exposed area of 1.33 cm^2 are contacted on the back side with a strip of aluminum foil and mounted in a Teflon etching cell; a platinum coil is used as the counter electrode. After etching, the surface of the wafer was rinsed with ethanol several times and dried under a dry nitrogen gas stream. Chemical oxidation of freshly etched PSi was performed by soaking the samples in a piranha solution (H_2SO_4:H_2O_2 in a 3:1 v/v proportion) (Frutarom, Israel and Carlo Erba Reagenti, Italy, respectively) for 12 h, followed by a thorough rinse with purified water.

Preparation of Porous SiO_2/poly(DMAEMA) Hybrids. Poly(DMAEMA) hydrogel was synthesized by a photopolymerization of DMAEMA monomer (Sigma Aldrich Chemicals) using polyethylene glycol (200) dimethacrylate (PEGDMA) (Polysciences, Inc. Warrington, PA, USA) as the cross-linking agent and 2,2-diethoxyacetophenone (DEAP) (Sigma Aldrich Chemicals) as the photoinitiator. Details on the composition of the pregel solution are summarized in Table S1 (of the Supporting Information). The pregel solution was prepared by dissolving the components in ethylene glycol (Carlo Erba Reagenti, Italy) at a constant molar ratio of DMAEMA:PEGDMA (35:1), followed by addition of 2 μL of 5% v/v DEAP in dimethyl sulfoxide (DMSO) (LobaChemie PVT. Ltd.) per 100 μL of the pregel solution. $PSiO_2$/poly(DMAEMA) hybrids were prepared by casting 50 μL of the pregel solution described above onto the $PSiO_2$ surface. The pregel solution was allowed to infiltrate into the porous nanostructure for 30 min and then spin-coated at 1000 rpm for 6 s to remove excess solution. The sample was covered with a polyester (Mylar) film and polymerization was initiated by illumination with UV light (at 365 nm, 0.7 mW cm^{-2}) for 15 min. The resulting hybrids were rinsed with purified water overnight to remove the unreacted species.

Optical Interference Spectroscopy. Interferometric reflectance spectra of the samples were collected using an Ocean Optics CCD USB 4000 spectrometer fitted with a microscope objective lens coupled to a bifurcated fiber optic cable. A tungsten light source was focused onto the center of the sample surface with a spot size of approximately 1−2 mm^2. Reflectivity data were recorded at a wavelength range of 400−1000 nm, with a spectral acquisition time of 100 ms. All data were recorded by Ocean Optics software and analyzed by Igor Pro software, version 6.0.3.0. Both illumination of the surface and detection of the reflected light were performed along an axis coincident with the surface normal.

pH-Dependent Behavior of Hybrids. Phosphate-buffered saline (PBS) 0.05 M were prepared by dissolving disodium hydrogen phosphate anhydrous (Carlo Erba Reagenti) and dihydrogen orthophosphate anhydrous (LobaChemie PVT Ltd.) in Milli-Q water with a pH ranging from 6 to 8. The ionic strength of buffer solutions was kept constant by addition of appropriate amounts of NaCl (Frutarom). pH cycling experiments were carried out by fixing the samples in a custom-made Plexiglas flow cell connected to a syringe pump. The hybrids were exposed to buffers with different pH values of 8, 7, and 6 (in this order), at a fixed flow rate of 0.5 mL s^{-1}. The pH was held constant for 10 min, after which a different buffer was introduced. Measurement of interferometric reflectance spectra was performed through a Plexiglas window ∼4 mm above the chip surface and the value of EOT was computed in real-time. Data points were collected every 20 s.

Preparation of the Biosensor. $PSiO_2$ was incubated with 3% v/v aqueous solution of 3-aminopropyltriethoxysilane (APTES) (Sigma Aldrich Chemicals) in double-distilled water for 30 min followed by extensive rinsing with purified water and ethanol. The resulting NH_2-modified $PSiO_2$ surface was exposed to a solution of 2.5 mg mL^{-1} of bis(*N*-succinimidyl)-carbonate (SC) (Sigma Aldrich Chemicals) in acetonitrile (Sigma Aldrich Chemicals) for 7 min, followed by subsequent rinsing with acetonitrile for 30 min. Next, the SC-modified $PSiO_2$ surface was reacted with 1 mg mL^{-1} of OPH (EC 3.1.8.1 Lybradyn, Inc. Oak Brook, IL) in PBS for 30 min, followed by subsequent rinsing steps in PBS, 1 M NaCl, and again PBS for 1 h. Synthesis of poly(DMAEMA) hydrogel within the porous nanostructure was carried out as we described earlier. The hydrogel was selectively synthesized in the center region of the $PSiO_2$ sample by exposure of an area of 0.2 cm^2 to UV illumination while the peripheral regions are masked with a printed polyester (Mylar) film. After polymerization, the resulting sample was thoroughly rinsed in water to remove any unreacted species.

High-Resolution Scanning Electron Microscopy and Energy Dispersive X-ray Spectroscopy. High-resolution scanning electron microscopy (HRSEM) studies were carried out using Carl Zeiss Ultra Plus instrument at an accelerating voltage of 1 keV. Energy dispersive X-ray spectroscopy (EDS)-coupled high-resolution scanning electron microscopy (HRSEM) of the neat $PSiO_2$ and hybrids was performed using a Carl Zeiss Ultra Plus instrument, at an accelerating voltage of 4 keV, using Espirit 1.8 software. Hybrids were prepared for observation by freeze fracturing the sample in liquid nitrogen followed by freeze-drying.

Infrared Spectroscopy. Surface modification of the PSi was characterized by attenuated total reflectance Fourier transform-infrared (ATR-FT-IR) spectroscopy. Spectra were recorded using a Thermo 6700 FTIR instrument equipped with a Smart iTR diamond ATR device. All samples were dried for 12 h in a vacuum oven at 25 °C prior to the FT-IR analysis.

Methyl Paraoxon Biosensing Experiments. Biosensors and control samples (i.e., $PSiO_2$/poly(DMAEMA) hybrids and OPH-functionalized $PSiO_2$) were incubated with different concentrations of methyl paraoxon (MOX) (Sigma Aldrich Chemicals) solutions in a flow cell setup. MOX solutions were prepared in 10 mM PBS with 0.1 mM $CoCl_2$ (Sigma Aldrich Chemicals), 5% v/v methanol (Gadot Ltd., Israel), and 150 mM NaCl. The MOX solution was introduced into the flow cell chamber while the reflectance spectra were continuously collected as described in previous sections. After attaining a constant EOT value, PBS was introduced to remove MOX remnants and enzymatic reaction products.

RESULTS AND DISCUSSION

Hybrid Preparation. The pH-responsive $PSiO_2$/poly(DMAEMA) hybrids are prepared by in situ polymerization of the pregel solution within the nanostructured $PSiO_2$ host. This inorganic porous substrate is fabricated by anodic electrochemical etching of a highly doped p-type Si wafer under a constant current density of 385 mA cm^{-2} for 30 s. The resulting PSi film is chemically oxidized with piranha solution to stabilize the porous layer and enhance the hydrophilicity of the porous scaffold. The $PSiO_2$ film is highly porous with an average total porosity of 80 ± 2%, as determined by gravimetric analysis. High-resolution scanning electron microscopy (HR-SEM) is used to characterize the porous layer thickness and morphology. The $PSiO_2$ film average thickness is 6800 ± 150 nm and its nanostructure is characterized by cylindrical

dx.doi.org/10.1021/ac4011815 | Anal. Chem. XXXX, XXX, XXX−XXX

interconnected pores of 60−100 nm in diameter, as depicted in Figure S1 of the Supporting Information.

Our previous work has demonstrated that incorporation of pH-responsive hydrogels [e.g., poly(NIPAM-*co*-acrylic acid)] within $PSiO_2$ hosts results in a hybrid nanomaterial with pH-responsive characteristics.[29] Herein, we use poly(DMAEMA)-based hydrogel, which is a weak polybase containing tertiary amine groups that undergo protonation at low pH.[60] As a result, the polymer chains become charged and therefore attract free counterions from the solution in order to maintain charge neutrality. The increased ion concentration inside the hydrogel gives rise to an osmotic pressure, which promotes an influx of water to the hydrogel network, resulting in a profound swelling of the hydrogel.[61,62] A pregel solution containing the monomer DMAEMA, polyethylene glycol dimethacrylate (PEGDMA) as the cross-linking agent, and 2,2-diethoxyacetophenone (DEAP) as the photoinitiator, is cast onto the $PSiO_2$ host. The pregel solution is allowed to infiltrate the porous nanostructure followed by UV polymerization, resulting in $PSiO_2$/poly-(DMAEMA) hybrids.

Characterization of pH-Responsivity of $PSiO_2$/Poly-(DMAEMA) Hybrids. The pH sensitivity of the $PSiO_2$/poly(DMAEMA) hybrids is characterized in real-time by monitoring the EOT changes upon exposure to buffers with different pH values. The hybrids are fixed in a custom-made flow cell assembly attached to a syringe liquid pump. The optical spectrum is continuously monitored, and the value of EOT is computed in real-time. Figure S2 of the Supporting Information shows a typical reflectance spectrum of the hybrid, depicting a Fabry−Pérot fringe pattern (Figure S2a) and the corresponding RIFTS spectrum (Figure S2b). First, the hybrid is conditioned by exposure to the flow of a pH 8 buffer for several hours. Then, buffers with pH values of 8, 7, and 6 are introduced for 10 min each. Figure 2 depicts time-resolved

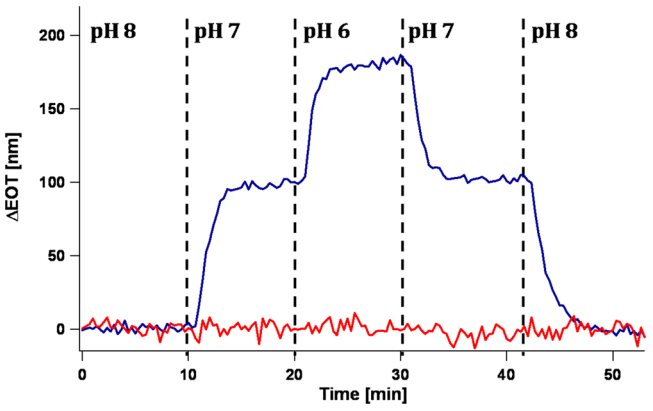

Figure 2. EOT changes of $PSiO_2$/poly(DMAEMA) hybrid (blue trace) and neat $PSiO_2$ (red trace) during pH cycling between 8 and 6. Samples are fixed in a flow cell assembly and exposed to a constant flow of 0.5 mL min^{-1} of the appropriate buffer. Positive values of ΔEOT indicate an increase in the value $2nL$.

normalized EOT changes (expressed as ΔEOT) of the $PSiO_2$/poly(DMAEMA) hybrid upon exposure to the different buffers. The hybrid demonstrates a significant increase in EOT as the pH value of a surrounding buffer decreases. ΔEOT values of approximately 100 and 80 nm are observed as the pH changes from 8 to 7 and from 7 to 6, respectively (Figure 2, blue trace). Complete recovery of the EOT to its initial value is recorded as the pH is cycled back from 6 to 7 and subsequently to 8. Moreover, the hybrid displays a rapid response to pH changes. It should be noted that recorded responses (∼1 min) include the time needed for the buffer to flow from its stock container to the flow cell chamber and the subsequent diffusion of the buffer into the hybrid. A control experiment with neat $PSiO_2$ film (no hydrogel) demonstrates a negligible response to the same temporal pH flux (see Figure 2, red trace).

Previous work on $PSiO_2$/poly(NIPAM-co-acrylic acid) established that EOT changes of the hybrid during pH cycling correlates with morphological changes due to the swelling/shrinking of the confined hydrogel phase of the hybrid.[29] Thus, the observed pH-dependent optical behavior of the $PSiO_2$/poly(DMAEMA) hybrid may be ascribed to the same phenomena. The increase in EOT upon pH decrease is mainly attributed to swelling of the poly(DMAEMA) hydrogel, resulting in the expansion of the entire hybrid in the direction perpendicular to the $PSiO_2/SiO_2$ interface, hence increasing the physical thickness of porous layer, L.[30,63] It should be emphasized that the $PSiO_2$ scaffold restricts the confined hydrogel swelling response. Our previous work showed that the hybrid response greatly depends upon the scaffold nanostructure characteristics, which dictates the confinement conditions of the hydrogel.[30] Upon pH increase, an opposite behavior (i.e., EOT decrease) is observed (Figure 2). This correlates to pH-induced shrinking of the confined poly(DMAEMA) hydrogel, leading to the reduction in the physical thickness of the hybrid. In addition, it is well-established that bulk hydrogel refractive index (n) decreases with swelling and vice versa.[64] Therefore, upon swelling/shrinking of the hydrogel, opposing changes in n and L values exert competing effects on the EOT of the hybrid.[29] Thus, the behavior of the $PSiO_2$/poly(DMAEMA) hybrid is well-described by models suggested in previous studies.[29,30,32]

Biosensor Design and Characterization. Previous sections have demonstrated that the new $PSiO_2$/poly-(DMAEMA) hybrids exhibit well-characterized, rapid, and reversible EOT changes in response to pH. These properties are crucial for the rational design of the current optical biosensing scheme.

Figure 3 schematically illustrates the synthetic steps followed to fabricate the biosensor. First, OPH is immobilized onto the $PSiO_2$ scaffold, as described in Figure 3 (panels a and b). The $PSiO_2$ is amino-silanized with 3-aminopropyltriethoxysilane (APTES) followed by incubation with bis(*N*-succinimidyl)-carbonate (SC). This homobifunctional cross-linker reacts with the surface amines through a nucleophilic attack of the amine on C═O succimide ester, eliminating one *N*-hydroxysuccinimide (NHS) group. The resulting NHS-modified surface is reacted with the OPH and conjugation is achieved via primary amine residues on the enzyme surface. Thus, the covalent immobilization of OPH upon the walls of $PSiO_2$ results in an array of interconnected nanoreactors for the hydrolysis of OPCs. Following OPH immobilization, the pH-responsive poly(DMAEMA) hydrogel is synthesized (Figure 3, panels c−e), as described in previous sections. The hydrogel is selectively synthesized in the center of the $PSiO_2$ sample, as depicted in Figure 3f, while the outer $PSiO_2$/OPH region remains intact (no hydrogel). The selective photopolymerization step confines the hydrogel synthesis to a predefined fraction of the pores. The resulting patterned hybrid region serves as the optical transducer element of the biosensor. The selective photopolymerization is important for maintaining the high enzymatic activity of the immobilized OPH, as during the hydrogel

dx.doi.org/10.1021/ac4011815 | *Anal. Chem.* XXXX, XXX, XXX−XXX

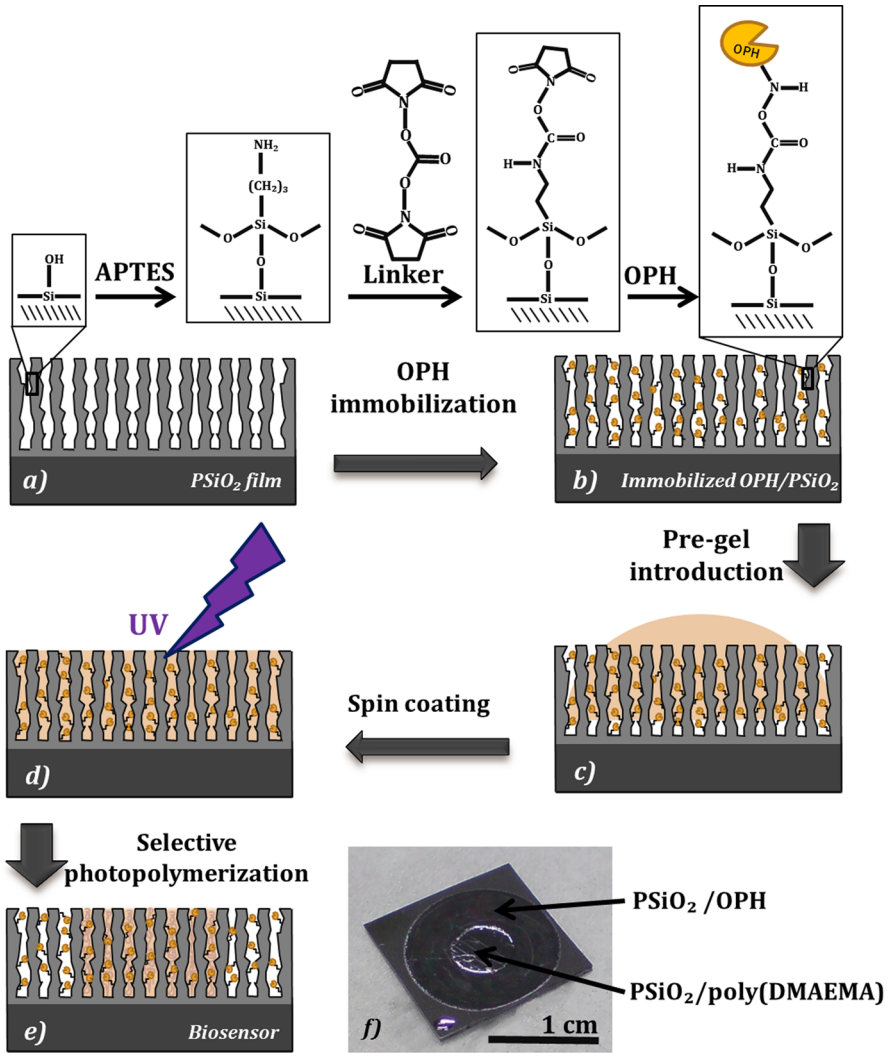

Figure 3. Schematic representation of (a–e) the preparation of the biosensor and (f) a photograph of the final biosensor. $PSiO_2$ is functionalized with OPH via surface chemistry. A pregel solution is cast and spin-coated onto the OPH-modified $PSiO_2$ sample. The $PSiO_2$ surface is masked with a polyester (Mylar) film, in which the periphery is printed to block UV and to prevent polymerization in this region. Photopolymerization is performed under a UV lamp at 356 nm for 15 min. The resulting biosensors are carefully soaked in PBS, rinsed thoroughly, and allowed to reach an equilibrium swelling state at room temperature. Note: These schematics are for illustration purposes only, as the hydrogel is also present to the top surface of the biosensor and OPH is conjugated to the top surface of the $PSiO_2$ layer.

synthesis chemical reactions between the different monomers and the enzyme can impair its catalytic function. The volume ratio between the $PSiO_2$/OPH compartment (in periphery) and the $PSiO_2$/poly(DMAEMA) hybrid (in center) is 6:1 (see Figure 3f). It is important to emphasize that the $PSiO_2$ is characterized by a network of interconnected pores,[14,65] allowing for efficient mass transfer between the two interfaced compartments of the biosensor.

Energy dispersive X-ray spectroscopy (EDS) coupled with HR-SEM is used to characterize the composition of the biosensor in order to confirm the presence of OPH and hydrogel within the $PSiO_2$ nanostructure. HR-SEM micrographs and corresponding EDS elemental maps (of Si, oxygen, and carbon) of both compartments of the biosensor (Figure S3, panels a and b, of the Supporting Information) show significantly higher carbon concentration within the porous layer in comparison to the neat $PSiO_2$ (Figure S3c of the Supporting Information), in which a significantly lower carbon signal is detected. These results are assigned to the presence of organic materials (i.e., hydrogel and OPH) throughout the entire depth of the porous layer[32] in both compartments of the biosensor. Thus, EDS analysis confirms that both hydrogel and enzymes penetrate and fill the pores; however, this technique lacks the ability to distinguish between the specific material composition of these two regions. In order to further confirm the selective hydrogel formation and enzyme immobilization within the different biosensor compartments, attenuated total reflectance Fourier transform infrared spectroscopy (ATR-FTIR) studies were performed (see the Supporting Information section for more details). The ATR-FTIR spectrum of the $PSiO_2$/OPH compartment in comparison to that neat $PSiO_2$ (Figure S4 of the Supporting Information) depicts two additional peaks (at 1645 cm^{-1} and 1543 cm^{-1}) that are attributed to the amide I and II bonds of the surface-bound enzyme, thus validating the presence of the OPH,[66] while the spectrum of the $PSiO_2$/poly(DMAEMA) compartment (Figure S4 of the Supporting Information), which contains both hydrogel and OPH, is dominated by characteristic peaks of the poly(DMAEMA) hydrogel. It is important to note that the ATR setup allows for a maximal penetration depth of ~2–3

dx.doi.org/10.1021/ac4011815 | Anal. Chem. XXXX, XXX, XXX–XXX

μm[67] and thus, the recorded spectra account only for the top porous layer and not the entire thickness of the film (~7 μm). Nevertheless, EDS results (Figure S3 of the Supporting Information) confirmed a homogeneous distribution of both C and O throughout the entire depth of the biosensor. Hence, the data from these two complementary techniques indicate that the poly(DMAEMA) hydrogel is selectively formed only within the predefined $PSiO_2$ volume and both poly(DMAEMA) and OPH are present throughout the entire depth of the porous layer.

Biosensing Experiments. To investigate the potential of this platform as an optical biosensor for the detection of OPCs, the sample is fixed in a flow cell setup and exposed to aqueous solutions of MOX. The reflectivity spectra from the $PSiO_2$/poly(DMAEMA) compartment is recorded in real-time throughout the experiment and the corresponding EOT values are computed. Prior to the introduction of MOX, the sample is preconditioned in PBS buffer to achieve a stable EOT baseline. Following this step, MOX (300 μM) is introduced, and the sample is incubated with the solution until the EOT signal stabilizes. Figure 4 displays the results of this experiment; the

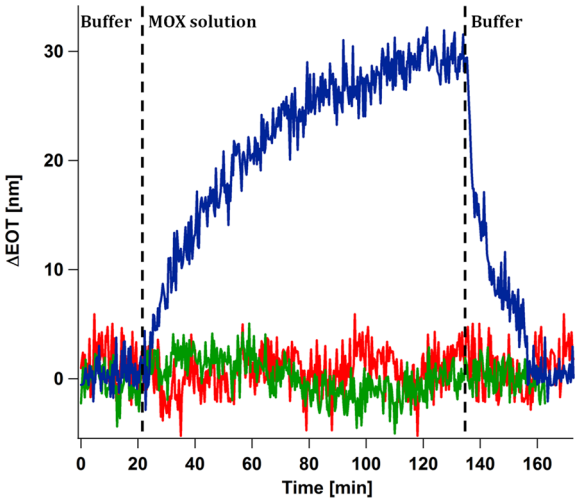

Figure 4. EOT changes during exposure to 300 μM MOX aqueous solution. Blue trace describes biosensor's response. Control samples of OPH-immobilized $PSiO_2$ [no poly(DMAEMA) hydrogel] and $PSiO_2$/poly(DMAEMA) hybrid (no OPH) are represented by red and green traces, respectively.

EOT (expressed as ΔEOT) rapidly increases with time, reaching a maximal value of 28 nm in less than two hours. In order to establish that the observed EOT changes result from the pH response of the $PSiO_2$/poly(DMAEMA) hybrid to the hydrolysis of MOX by the immobilized OPH, proper control experiments are carried out. Therefore, the optical response of OPH-modified $PSiO_2$ and $PSiO_2$/poly(DMAEMA) hybrid samples subjected to similar experimental conditions is monitored. Both samples exhibit negligible EOT changes upon the introduction of MOX (Figure 4). The lack of optical response from the OPH-modified $PSiO_2$ sample indicates that the refractive index changes, which occur during MOX solution introduction and subsequent MOX degradation, are undetectable by RIFTS. As for the hybrid behavior, it can be concluded that exposure to MOX does not induce volume changes of the hydrogel, which may facilitate the optical response.[29] Thus, these control experiments confirm that the EOT shift of the biosensor system can be ascribed to the swelling of the $PSiO_2$/poly(DMAEMA) hybrid and not to differences in the refractive index values of the media. Furthermore, interfacing the two compartments (i.e., $PSiO_2$/OPH and $PSiO_2$/poly(DMAEMA)) is crucial for the biosensor function.

As the MOX is degraded within the $PSiO_2$/OPH compartment, the products of this hydrolysis reaction lower the pH of the surrounding solution. The interconnected porous nanostructure[65] allows for protons (MOX hydrolysis products) to diffuse to the hybrid region and to trigger the swelling of the poly(DMAEMA) hydrogel. Nevertheless, we cannot rule out the transport of enzymatic products from the $PSiO_2$/OPH compartment to the surrounding buffer solution and then their diffusion into the neighboring hybrid sections. The $PSiO_2$/poly(DMAEMA) hybrid response to this local pH change results in an EOT increase, as demonstrated in section 2.2 and Figure 2.

The response time of the biosensor is combined from the following steps that occur simultaneously: (i) diffusion of the MOX substrate into the $PSiO_2$/OPH compartment, (ii) enzymatic degradation of MOX by the immobilized OPH, (iii) diffusion of the reaction products from the $PSiO_2$/OPH chamber into the $PSiO_2$/poly(DMAEMA) hybrid, (iv) volume change of the hybrid in response to pH change, which in turn induces the observed EOT shifts. The rapid hybrid optical response, observed in Figure 2, suggests that the diffusion and enzymatic reaction, which are interrelated, are the limiting steps in this biosensing scheme. Thus, from a practical point of view, the initial optical response of the biosensors (within minutes, see Figure 4) qualitatively confirms that the studied solution is indeed contaminated with MOX. Nevertheless, in order to quantify MOX concentration (as will be discussed in the following sections), reaching a steady-state optical response is required (~2 h for 300 μM MOX).

Upon reaching a steady-state response of the biosensor, the cell is rinsed by a flow of PBS to remove the MOX remnants and the enzymatic reaction products. The ΔEOT is observed to rapidly decrease, see Figure 4, reaching its original value within several minutes. As the MOX hydrolysis products are replaced with the fresh buffer, the tertiary amine group of the poly(DMAEMA) are deprotonated, resulting in water expulsion and hydrogel shrinkage to its initial state. Thus, the biosensor behavior is fully reversible, and it can easily be regenerated for consecutive biosensing analysis.

The dynamic range of the biosensor was studied by exposing the biosensor to a set of MOX solutions with different concentrations (50−1000 μM). Figure 5 summarizes the results of these experiments, depicting the maximal ΔEOT value attained for each MOX concentration. The Δ*E*OT is found to be proportional to the MOX concentration, displaying a very good linearity (R^2 = 0.98) of the optical response of the biosensor to the analyte concentration. On the basis of these results, the detection limit of the biosensor was calculated to be 40 μM.

Current experiments in our lab are aimed at improving the sensitivity of the biosensor and enhancing its response time by optimizing the fabrication $PSiO_2$/poly(DMAEMA) hybrid to increase the interface of the two interacting compartments.

CONCLUSIONS

A new pH-responsive $PSiO_2$/poly(DMAEMA) hybrid was synthesized and characterized in terms of its optical response to pH changes. The hybrid displays well-defined, rapid, and

dx.doi.org/10.1021/ac4011815 | Anal. Chem. XXXX, XXX, XXX−XXX

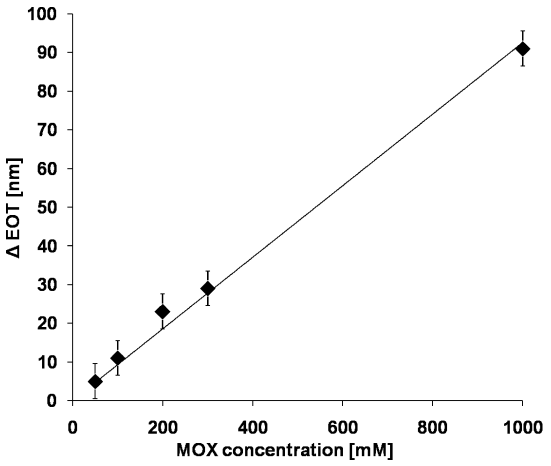

Figure 5. EOT changes of the biosensor vs different MOX concentrations.

reversible EOT changes. The magnitude of optical response to pH changes is significantly higher in comparison to previous $PSiO_2$ hybrids.[29] These advantageous properties allow for the application of this new hybrid in different biosensing schemes. To demonstrate this concept, we design and fabricate a bifunctional nanostructured platform for label-free optical detection and quantification of OPCs in aqueous solutions. The biosensor is constructed from two conjugated interacting compartments (i.e., the pH-responsive $PSiO_2$/poly-(DMAEMA) hybrid and $PSiO_2$/OPH). The pH-responsive hybrid compartment functions as the optical transducer element. While, the OPH-modified $PSiO_2$ region, which functions as an array of nanoreactors for the hydrolysis of the OPC, serves as the biorecognition element of the biosensor. Exposure to the target analyte results in a rapid and reproducible change in the optical reflectivity spectrum of the hybrid, allowing for a label-free detection and quantification of OPCs in a simple and reliable manner within tens of minutes. The linearity of the biosensor within its dynamic range (50–1000 μM) is demonstrated. Moreover, the biosensor can easily be regenerated by a short rinsing step for multiple biosensing analyses.

■ ASSOCIATED CONTENT

Ⓢ Supporting Information

Additional information as noted in text. This material is available free of charge via the Internet at http://pubs.acs.org.

■ AUTHOR INFORMATION

Corresponding Author

*E-mail: esegal@tx.technion.ac.il. Tel: +972-4-8295071. Fax: +972-4-8293399.

Author Contributions

The manuscript was written through contributions of all authors. All authors have given approval to the final version of the manuscript.

Notes

The authors declare no competing financial interests.

■ ACKNOWLEDGMENTS

This work was supported by the Technion Funds for Security Research and by the Israeli Ministry of Science (Grant 3-6798). We thank Giorgi Shtenberg, Dr. Naama Massad-Ivanir, Tal Ziedman, and Dr. Lisa M. Bonanno for helpful discussions and comments.

■ REFERENCES

(1) Lin, V. S. Y.; Motesharei, K.; Dancil, K. P. S.; Sailor, M. J.; Ghadiri, M. R. *Science* **1997**, *278*, 840–843.
(2) Li, Y. Y.; Cunin, F.; Link, J. R.; Gao, T.; Betts, R. E.; Reiver, S. H.; Chin, V.; Bhatia, S. N.; Sailor, M. J. *Science* **2003**, *299*, 2045–2047.
(3) Orosco, M. M.; Pacholski, C.; Sailor, M. J. *Nat. Nanotechnol.* **2009**, *4*, 255–258.
(4) Jane, A.; Dronov, R.; Hodges, A.; Voelcker, N. H. *Trends Biotechnol.* **2009**, *27*, 230–239.
(5) Bocking, T.; Kilian, K. A.; Gaus, K.; Gooding, J. J. *Adv. Funct. Mater.* **2008**, *18*, 3827–3833.
(6) Bonanno, L. M.; Segal, E. *Nanomedicine* **2011**, *6*, 1755–1770.
(7) Weiss, S. M.; Rong, G.; Lawrie, J. L. *Phys E (Amsterdam, Neth.)* **2009**, *41*, 1071–1075.
(8) Ouyang, H.; DeLouise, L. A.; Miller, B. L.; Fauchet, P. M. *Anal. Chem.* **2007**, *79*, 1502–1506.
(9) Bonanno, L. M.; DeLouise, L. A. *Biosens. Bioelectron.* **2007**, *23*, 444–448.
(10) Sailor, M. J.; Link, J. R. *Chem. Commun. (Cambridge, U.K.)* **2005**, 1375–1383.
(11) Bonanno, L. M.; DeLouise, L. A. *Adv. Funct. Mater.* **2010**, *20*, 573–578.
(12) Kilian, K. A.; Boecking, T.; Gooding, J. J. *Chem. Commun. (Cambridge, U.K.)* **2009**, 630–640.
(13) Massad-Ivanir, N.; Shtenberg, G.; Segal, E. *Nano-Biotechnology for Biomedical and Diagnostic Research*; Zahavy, E., Ordentlich, A., Yitzhaki, S., Shafferman, A., Eds.; Springer: The Netherlands, 2012, Vol. *733*, 37–45.
(14) Bisi, O.; Ossicini, S.; Pavesi, L. *Surf. Sci. Rep.* **2000**, *38*, 1–126.
(15) Gurtner, C.; Wun, A. W.; Sailor, M. *Angew. Chem., Int. Ed.* **1999**, *38*, 1966–1968.
(16) Buriak, J. M.; Stewart, M. P.; Geders, T. W.; Allen, M. J.; Choi, H. C.; Smith, J.; Raftery, D.; Canham, L. T. *J. Am. Chem. Soc.* **1999**, *121*, 11491–11502.
(17) Janshoff, A.; Dancil, K. P. S.; Steinem, C.; Greiner, D. P.; Lin, V. S. Y.; Gurtner, C.; Motesharei, K.; Sailor, M. J.; Ghadiri, M. R. *J. Am. Chem. Soc.* **1998**, *120*, 12108–12116.
(18) Robins, E. G.; Stewart, M. P.; Buriak, J. M. *Chem. Commun. (Cambridge, U.K.)* **1999**, 2479–2480.
(19) Kilian, K. A.; Boecking, T.; Gaus, K.; Gal, M.; Gooding, J. J. *ACS Nano* **2007**, *1*, 355–361.
(20) Mun, K. S.; Alvarez, S. D.; Choi, W. Y.; Sailor, M. J. *ACS Nano* **2010**, *4*, 2070–2076.
(21) Pacholski, C.; Sartor, M.; Sailor, M. J.; Cunin, F.; Miskelly, G. M. *J. Am. Chem. Soc.* **2005**, *127*, 11636–11645.
(22) Massad-Ivanir, N.; Shtenberg, G.; Zeidman, T.; Segal, E. *Adv. Funct. Mater.* **2010**, *20*, 2269–2277.
(23) Massad-Ivanir, N.; Shtenberg, G.; Tzur, A.; Krepker, M. A.; Segal, E. *Anal. Chem.* **2011**, *83*, 3282–3289.
(24) Elliott, J. E.; Macdonald, M.; Nie, J.; Bowman, C. N. *Polymer* **2004**, *45*, 1503–1510.
(25) Hirokawa, Y.; Tanaka, T. *J. Chem. Phys.* **1984**, *81*, 6379–6380.
(26) Jin, S. P.; Liu, M. Z.; Zhang, F.; Chen, S. L.; Niu, A. Z. *Polymer* **2006**, *47*, 1526–1532.
(27) Jin, X.; Hsieh, Y. L. *Polymer* **2005**, *46*, 5149–5160.
(28) Tanaka, T.; Nishio, I.; Sun, S. T.; Uenonishio, S. *Science* **1982**, *218*, 467–469.
(29) Perelman, L. A.; Moore, T.; Singelyn, J.; Sailor, M. J.; Segal, E. *Adv. Funct. Mater.* **2010**, *20*, 826–833.
(30) Segal, E.; Perelman, L. A.; Cunin, F.; Di Renzo, F.; Devoisselle, J. M.; Li, Y. Y.; Sailor, M. J. *Adv. Funct. Mater.* **2007**, *17*, 1153–1162.
(31) Wu, J.; Sailor, M. *Adv. Funct. Mater.* **2009**, *19*, 733–741.
(32) Massad-Ivanir, N.; Friedman, T.; Nahor, A.; Eichler, S.; Bonanno, L. M.; Sa'ar, A.; Segal, E. *Soft Matter* **2012**, *8*, 9166–9176.
(33) McInnes, S. J. P.; Voelcker, N. H. *Future Med. Chem.* **2009**, *1*, 1051–1074.

(34) Hopkins, E. H.; Hippe, D. J.; Frick, E. A.; Bluell, G. R. *Organophosphorus Pesticide Occurrence and Distribution in Surface and Ground Water of the United States 1992−1997*; U.S. Geological Survey Open-File Report 00-187; USGS: Reston, VA, 2000.
(35) Grimsley, D. K.; Disioudi, B. D.; Holton, T. D.; Sacchettini, J. C.; Wild, J. R. In *Enzymes in Action Green Solutions for Chemical Problems*; Zwanenburg, W., Mikolajczyk, M., Kielbasinski, P., Eds.; Kluwer Academic: Dordrecht, 2000; Vol. *33*, 223−242.
(36) Noort, D.; Benschop, H. P.; Black, R. M. *Toxicol. Appl. Pharmacol.* **2002**, *184*, 116−126.
(37) Bajgar, J. *Advances in Clinical Chemistry*; Academic Press: San Diego, 2004; *38*, 151216.
(38) Munnecke, D. M. *J. Agric. Food Chem.* **1980**, 105−111.
(39) Donarski, W. J.; Dumas, D. P.; Heitmeyer, D. P.; Lewis, V. E.; Raushel, F. M. *Biochemistry* **1989**, *28*, 4650−4655.
(40) Mulchandani, P.; Chen, W.; Mulchandani, A. *Environ. Sci. Technol.* **2001**, *35*, 2562−2565.
(41) Walker, J. P.; Kimble, K. W.; Asher, S. A. *Anal. Bioanal. Chem.* **2007**, *389*, 2115−2124.
(42) Mulchandani, P.; Mulchandani, A.; Kaneva, I.; Chen, W. *Biosens. Bioelectron.* **1999**, *14*, 77−85.
(43) Flounders, A. W.; Singh, A. K.; Volponi, J. V.; Carichner, S. C.; Wally, K.; Simonian, A. S.; Wild, J. R.; Schoeniger, J. S. *Biosens. Bioelectron.* **1999**, *14*, 715−722.
(44) Mulchandani, A.; Mulchandani, P.; Kaneva, I.; Chen, W. *Anal. Chem.* **1998**, *70*, 4140−4145.
(45) Orbulescu, J.; Constantine, C. A.; Rastogi, V. K.; Shah, S. S.; DeFrank, J. J.; Leblanc, R. M. *Anal. Chem.* **2006**, *78*, 7016−7021.
(46) Russell, R. J.; Pishko, M. V.; Simonian, A. L.; Wild, J. R. *Am. Chem. Soc., Abstr. Pap.* 2000, *219*, ANYL 146.
(47) Fitch, J. P.; Raber, E.; Imbro, D. R. *Science* **2003**, *302*, 1350−1354.
(48) Wang, J.; Chen, G.; Muck, A., Jr.; Chatrathi, M. P.; Mulchandani, A.; Chen, W. *Anal. Chim. Acta* **2004**, *505*, 183−187.
(49) Witkiewicz, Z.; Mazurek, M.; Szulc, J. *J. Chromatogr.* **1990**, *503*, 293−357.
(50) Zaugg, S.; Sandstorm, M.; Smith, S.; Fehlberg, K. *Methods of Analysis by the U.S. Geological Survey National Water Quality Laboratory−Determination of Pesticides in Water by C-18 Solid-Phase Extraction and Capillary-Column Gas Chromatography/Mass Spectrometry with Selected-Ion Monitoring*; U.S. Geological Survey Open-File Report 95-181; USGS: Reston, VA, 1995.
(51) Rogers, K. R.; Wang, Y.; Mulchandani, A.; Mulchandani, P.; Chen, W. *Biotechnol. Prog.* **1999**, *15*, 517−521.
(52) Kientz, C. E. *J. Chromatogr., A* **1998**, *814*, 1−23.
(53) Bachmann, T. T.; Leca, B.; Vilatte, F.; Marty, J. L.; Fournier, D.; Schmid, R. D. *Biosens. Bioelectron.* **2000**, *15*, 193−201.
(54) Liu, G. D.; Lin, Y. H. *Anal. Chem.* **2006**, *78*, 835−843.
(55) Singh, A. K.; Flounders, A. W.; Volponi, J. V.; Ashley, C. S.; Wally, K.; Schoeniger, J. S. *Biosens. Bioelectron.* **1999**, *14*, 703−713.
(56) Skladal, P. *Anal. Chim. Acta* **1992**, *269*, 281−287.
(57) Ju, H.; Zhang, X.; Wang, J. In *NanoBiosensing: Principles, Development and Application*; Springer: New York, 2011; 365−391.
(58) Dumas, D. P.; Caldwell, S. R.; Wild, J. R.; Raushel, F. M. *J. Biol. Chem.* **1989**, *264*, 19659−19665.
(59) Lei, Y.; Mulchandani, P.; Wang, J.; Chen, W.; Mulchandani, A. *Environ. Sci. Technol.* **2005**, *39*, 8853−8857.
(60) Amalvy, J. I.; Wanless, E. J.; Li, Y.; Michailidou, V.; Armes, S. P.; Duccini, Y. *Langmuir* **2004**, *20*, 8992−8999.
(61) Tokarev, I.; Minko, S. *Soft Matter* **2009**, *5*, 511−524.
(62) Schepelina, O.; Poth, N.; Zharov, I. *Adv. Funct. Mater.* **2010**, *20*, 1962−1969.
(63) Populaire, C.; Remaki, B.; Lysenko, V.; Barbier, D.; Artmann, H.; Pannek, T. *Appl. Phys. Lett.* **2003**, *83*, 1370−1372.
(64) Hiltner, P. A.; Krieger, I. M. *J. Phys. Chem.* **1969**, *73*, 2386−&.
(65) Zhang, X. G. *J. Electrochem. Soc.* **2004**, *151*, C69−C80.
(66) Socrates, G. *Infrared and Raman Characteristics Group Frequencies*; Wiley : Hoboken, NJ, 2001.
(67) Larkin, P. J. *Infrared and Raman Spectroscopy: Principles and Spectral Interpretation*, Elsevier: Amsterdam, 2011.